

Development of Non-Intensified Charge-Coupled Device Area X-ray Detectors

N. M. Allinson

Department of Electronics, University of York, York YO1 5DD, UK

(Received 12 April 1994; accepted 9 June 1994)

Area X-ray detectors based on charge-coupled device imagers can provide excellent performance in terms of spatial resolution, sensitivity and dynamic range. Improvements in the fabrication of the primary converter, either scintillator or phosphor, mean that it is becoming possible to dispense with prestorage intensifiers and still provide outstanding low-level signal performance. Structured CsI scintillators are presented as one method of providing high efficiency and excellent spatial resolving power for this primary converter. Characterization of detector performance, in terms of such parameters as the detective quantum efficiency, point-spread function and dynamic range, needs to be directly related to the specific application of the detector. This contribution emphasizes the interplay of these parameters in the optimum design of detector systems. Performance prediction, based on measurements taken from prototype development systems, illustrates how such detectors will meet the exacting requirements of macromolecular crystallography.

Keywords: X-ray detectors; charge-coupled devices; detective quantum efficiency; point-spread function; macromolecular crystallography.

1. Introduction

Detector design is the technology of compromise. Though it is possible to imagine an ideal detector – one that detects all incident photons, introduces no noise components, exhibits an infinite dynamic range and possesses zero readout time – it is impossible to even consider constructing one. There are a myriad of constraints imposed upon the designer: some are due to fundamental physical limitations; some are due to the non-availability of suitable materials and components; and some are more prosaic and are related to cost. Some constraints mutually conflict with each other. It is generally not possible for a detector system to have optimum performance for very low-level signals and yet possess a high dynamic range. Measurement accuracy and readout speed are inversely related. However, it is possible that, given a particular application with its own set of requirements, an optimum detector system can be successfully designed and constructed.

This paper will concentrate on the design of charge-coupled device (CCD)-based area detectors for macromolecular crystallography. Our current approach, and one being pursued by a small number of groups across the world (Phillips, Stanton, O'Mara, Naday & Westbrook, 1993; Eikenberry, Tate, Bilderback & Gruner, 1992), is based on the exploitation of the excellent properties of scientific grade CCD imagers coupled *via* an optical relay, using a fibre-optic taper, to the initial conversion element – an X-ray-sensitive phosphor or scintillator.

2. Macromolecular crystallography requirements

The detector requirements for macromolecular crystallography (see, for example, Helliwell, 1992) are fairly exacting

with a primary need to record, with high precision, the integrated spot intensities of dense diffraction patterns. For routine data collection, the need is to record a complete data set in as short a time as possible (bearing in mind the prerequisite for accurate measurements) so that radiation damage to the crystal is minimized. There is a large range of intensities in diffraction patterns, but detector integration time is determined primarily by the need to obtain satisfactory counting statistics for weak spots, usually at high diffraction angles. The inclusion of these weak spots not only determines the efficiency of the detector for low-level signal operation but also the size of its active aperture. Large size is also important since the background scatter follows an inverse-square law whilst the diffracted photons are collimated. With these general comments in mind, it is possible to develop a functional detector specification for use in most routine diffraction experiments at synchrotron sources.

(a) Aperture size – 150 × 150 mm as a minimum for a normal beam geometry; preferably 250 × 250 mm.

(b) Resolution – typically 200 resolvable diffraction orders per radial scan (measured at a separation of 1% of spot peak levels). A spot integration region (boxel) of 5 × 5 pixels is normally used to provide spot profiling.

(c) Tessellation – typically 2000 × 2000 pixels, increasing to 4000 × 4000 pixels for Laue diffraction. With the use of 200–500 μm diameter collimators (dictated by crystal dimensions) and the boxel size mentioned above, this implies an individual pixel dimension of 40–100 μm square.

(d) Efficiency – it is normal to quote efficiency in terms of the detective quantum efficiency (DQE) of the complete detecting system. As the following sections demonstrate,

DQE is not a simple quantity to specify for a practical detection system. The efficiency should be sufficient to permit the recording of weak diffraction spots (say, 50 photons integrated intensity) at a minimum accuracy of 25% in a realistic integration time over the energy range of interest. A simplistic application of the expression for DQE, namely

$$\text{DQE} = (S_0/\sigma_0)^2 / (S_i/\sigma_i)^2 \quad (1)$$

would, therefore, imply a minimum DQE of approximately 50% for these weak spots.

(e) Global count rate – for current synchrotron beamlines, a rate in excess of 5×10^6 photons s^{-1} is required, but for third-generation synchrotron sources this limit may be more realistically set at 10^8 photons s^{-1} .

(f) Local count-rate – for current beamlines, the limit should be $> 10^4$ photons s^{-1} , with a projected requirement of up to 5×10^5 photons s^{-1} .

(g) Energy range – 2 to 35 keV, with a more typical range of 8–17 keV.

(h) Frame rate – for conventional crystallography, minimum integration times of 5–10 s could be expected, with a minimum of about 1 s increasing to several minutes for virus experiments. In order to reduce the total data-collection time, the duty cycle of the detecting system should be high, and this implies a frame readout time of less than 1 s.

(i) Dynamic range – typically at least $10^3:1$. Dynamic range can be defined in a number of ways and this is discussed further in §4.3.

(j) Other factors – these include linearity of response throughout the usable dynamic range, uniformity of response over the active aperture, high stability of response over time (to minimize the number of calibration runs) and of geometric distortions of the detected image. It is more difficult to assign precise specifications to these factors, but we can be guided by the need for 1–2% statistics on intensity and geometric prediction of spot coordinates to be good to less than one pixel.

3. System topologies

Scientific grade area CCDs (Janesick & Elliott, 1992) are available from a number of manufacturers with pixel numbers of up to 4000×4000 , although 1000×1000 is more typical. The individual photosite dimensions are usually in the range 10–30 μm square. The inherent sensitivity of the CCD over other imaging devices arises from its very low readout capacitance. For an output-node capacitance of 0.1 pF, the voltage sensitivity is 1.6 μV per transferred electron. With relatively slow readout rates and device cooling, the noise floor is typically a few electrons r.m.s.; and the saturation limit (*i.e.* full-well capacity) can approach 10^6 electrons. Conventional scientific grade CCDs are full-frame devices, which means there is no separate shielded storage region and this implies the closure of an external mechanical shutter (though image intensifiers can be used as fast electronic shutters) during the readout period of the integrated image. CCDs can either be front

illuminated (*i.e.* photons are incident on the device surface that is overlaid with the transfer and storage-gate electrode structure) or back illuminated (*i.e.* the bulk of the underlying Si substrate is removed and photons are incident on the rear surface of the device). Back-illuminated devices generally possess improved imaging qualities (*e.g.* up to 60% higher sensitivity over parts of the visible spectral range) but they, in the past, have usually demanded a much higher price. The worldwide investment over three decades in Si-based CCDs (and more generally in microelectronics) has resulted in very high quality cost-effective devices with no or very few defects – even for devices that occupy several square centimetres of Si.

The four basic system topologies are illustrated in Fig. 1. Systems that employ prestorage-gain elements will not be considered in this paper, but details are given by Arndt (1986, 1990), Gruner (1989) and Amemiya *et al.* (1994). Before discussing the components of the more conventional approach of employing a scintillator or phosphor as the primary converter, it is appropriate to consider direct detection using CCDs.

3.1. Direct detection

The sole detection process in the soft X-ray region is the interaction of an incident photon with an inner-shell electron, and for solid-state detectors this absorption is accompanied by the generation of electron–hole pairs. Only about one third of the deposited energy is employed in creating these pairs. The internal gain, or ideal quantum yield η_i , for Si is given by,

$$\eta_i = E_\lambda / 3.65, \quad (2)$$

where E_λ is the energy (eV) of the incident X-rays. This high gain, resulting in approximately 2000 electron–hole pairs for a single 8 keV photon, is an advantage in energy discriminating applications for isolated event detection. For integrating detectors, where the incident flux may be high, there are serious limitations in the available dynamic range due to CCD saturation effects. The useful X-ray energy range, over which the detection efficiency is high, is based

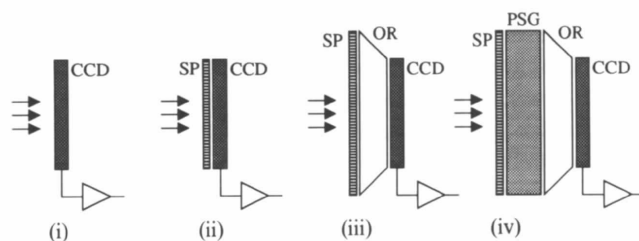


Figure 1

Basic detector topologies, (i) CCD direct detection; (ii) scintillator/phosphor directly coated on CCD; (iii) scintillator/phosphor screen, with lens or fibre-optic coupling to CCD; (iv) scintillator/phosphor screen coupled to image intensifier or microchannel plate coupled *via* optical relay to CCD. CCD, CCD imager; SP, scintillator or phosphor; OR, optical relay; PSG, prestorage gain.

around the Si *K*-edge ($E_i = 1.84$ keV) and extends from 0.5 to 30 keV for devices with depletion-layer depths in the 150–300 μm range. Over this range the detection efficiency will be in excess of 20% and may approach 100%. The high quality of diffraction data obtainable using direct detection with high-resistivity devices has been demonstrated (Allinson *et al.*, 1989), and the narrow point-spread function remains a benchmark for other possible schemes. Direct detection not only offers excellent resolution but can also overcome possible temporal problems associated with phosphor conversion and is useful, therefore, for time-resolved applications (Allinson *et al.*, 1992). The high internal gain relaxes the demands on low-noise amplification of the output signals and device cooling.

The concerns over possible radiation damage to the detector itself are not as serious as most of the literature would suggest, as most investigations have considered very high energy radiation (> 60 keV). Extensive investigations of radiation damage in the CCD have shown that this is primarily due to the trapping of photo-generated holes in existing defects at or near the Si–SiO₂ interface (Magorrian & Allinson, 1988). This damage manifests itself primarily as an increase in the device's dark current (with lesser effects in the form of reduced charge-transfer efficiency and voltage level shifts). A typical accumulated radiation dose, before the device becomes unusable, is, for a front-illuminated CCD, about 5×10^6 rad (Si). The damage can be completely annealed by warming the affected devices in a hydrogen-rich atmosphere (Allinson, Allsopp, Quale & Magorrian, 1991).

The particular properties of direct detection can mean that it is the optimum approach for certain applications. The limited size of CCDs, or other Si-based detectors, means that providing active apertures up to 600 cm² is both difficult and expensive. Mosaics of tiled CCDs are possible, as a small number of CCDs are designed to be edge buttable along two or three sides of the Si die. A stripe at least 200 μm wide at the butted edges will be effectively unusable, and it is not possible to construct contiguous mosaics more than two CCDs deep.

3.2. Primary conversion

Though there is no fundamental difference in the physical processes involved in wavelength conversion for phosphors or scintillators, it is useful to categorize phosphors as powder-based layers and scintillators as vapour deposited with some degree of crystal structure. The essential requirements of both are as follows.

(a) High conversion efficiency from X-ray photons to visible photons.

(b) High X-ray absorption or stopping power.

(c) Good spectral match of the light emission with the spectral response of the subsequent stages (*i.e.* intensifier photocathode, or optical relay and CCD).

(d) High spatial resolution.

(e) Prompt emission of light with any persistence effects below levels of interest (*i.e.* no memory effects).

Table 1

Common phosphor characteristics based on Gruner *et al.* (1993).

Phosphor	Efficiency*	Decay time†	Stopping power for 10 mg cm ⁻² layer		
			5.9 keV	8.1 keV	1.36 keV
Y ₂ O ₂ S:Tb	50–140	—	0.92	0.65	0.23
Y ₂ O ₂ S:Eu	130–150	—	0.92	0.65	0.23
La ₂ O ₂ S:Eu	170	300 ms	1.00	0.95	0.54
Gd ₂ O ₂ S:Tb	50–70	10 ms	0.91	0.97	0.66

* Measured as photons per ⁵⁵Fe X-ray photon, and transmitted through a fibre-optic plate. † Measured to 0.2% of peak intensity level.

(f) High linearity of light output with incident X-ray flux.

(g) High uniformity over the entire aperture.

(h) Highly robust and stable (*e.g.* unaffected by the atmosphere, radiation hard).

Over a dozen inorganic materials have been employed as X-ray phosphors, with the most popular being Gd₂O₂S:Tb and Y₂O₂S (doped with Tb or Eu). There is no 'ideal' phosphor as, for example, Y-based phosphors exhibit a higher efficiency than Gd-based ones, but the Y *K*-edge at 17 keV limits their useful range to below about 12 keV. Gruner, Barna, Wall, Tate & Eikenberry (1993) have provided a recent review of their extensive investigations into powder phosphors on which Table 1 is based.

We have concentrated on the development of structured scintillator screens using doped CsI. Doped CsI possesses a number of useful properties. It has a high density (~ 4.5 g cm⁻³), is relatively non-hygroscopic, has a fast response with no long-lived scintillator components above the 0.01% of peak level, and a high DQE up to approximately 35 keV. It can easily be evaporated onto glass and other substrates, and under the appropriate conditions will grow into thin needle-shaped crystallites orthogonal to the substrate (Ito, Yamaguchi & Oba, 1987). CsI doped with Tl is preferred to Na doping, as light emission of the former ($\lambda_{\text{max}} = 540$ nm) is better matched to the spectral sensitivity of the CCD. The spatial resolution of any scintillator or phosphor is limited by the scattering of the emitted light as it passes through the material. To preserve the inherent resolution of the underlying coherent fibre-optic bundle, the cladding glass around each individual fibre is preferentially etched to leave an array of exposed cores (typically 5 μm diameter). The surface is then further prepared before CsI is directly evaporated. The CsI grows as extensions of these isolated pillars so that the scintillator light is efficiently transferred to the fibre optics with minimal cross-talk (Castelli, Allinson, Moon & Watson, 1994). Spatial resolution of a detector system is usually expressed in terms of the point-spread function (PSF). This is further discussed in §4.2 as it has a major effect on DQE at low intensity levels. The usual measurement technique is to employ a metal mask containing a grid of many small holes, and the entire mask is illuminated by a spatially uniform X-ray flux. A large number of the resulting image spots are cylindrically averaged to form an average spot which is then deconvolved to yield the PSF. Radially integrating the PSF yields

the integrated-charge collection efficiency, which shows directly the fraction of the integrated charge that is accumulated as a function of pixel radius (for an ideal system, all the charge for one spot should be collected in the centre pixel). Fig. 2 shows the measured integrated-charge collection profiles for both structured and uniform 30 μm CsI(Tl) layers grown directly on a fibre-optic faceplate. This figure also shows the charge spreading due solely to the fibre optics and CCD (measured using visible light). This indicates that there is little image degradation due to the structured scintillator. For the structured scintillator 70% of the induced charge is contained within a two pixel radius compared with a 15 pixel radius for the unstructured scintillator (for the optics and CCD alone this percentage is attained in a one pixel radius). For the prototype system described later, a 30 μm CsI(Tl) scintillator yields a detected signal of ~ 30 e per detected 8 keV photon. The front surface of the scintillator can be coated with a very thin reflecting aluminized mylar film, which not only hermetically seals the scintillator but also increases the overall efficiency by redirecting any efferent scintillator light.

3.3. Prestorage gain

The function of a prestorage-gain element – image intensifier or micro-channel plate – is to improve low-level signal detection. It can also act as a demagnifier and so matches the active aperture size to the more restricted size of the CCD. It is useful to consider the need for prestorage gain if the initial efficiency of the primary converter is sufficiently high. Also, the demagnification function can be satisfied separately using a fibre-optic taper.

Noise sources within a detector system can be characterized into three main types.

Type 1 – signal-dependent noise which is due to the random nature of any conversion or attenuation process. Each such process can be considered as an independent random process. The noise figure, F , of each process is given by

$(\text{SNR}_i)^2/(\text{SNR}_o)^2$, where SNR_i and SNR_o are the signal-to-noise ratios at the input and output of each process, respectively. The overall noise figure of n cascaded processes (Arbel, 1980) can be expressed as,

$$F = F_1 + [(F_2 - 1)/P_1] + \dots + [(F_n - 1)/\prod_{i=1}^{n-1} P_i], \quad (3)$$

where P_i is the signal gain (or attenuation) associated with the i th process. From this expression it can be seen that the overall noise figure always degrades as the number of processes increases and that a high gain for the initial process is essential for good overall noise performance.

Type 2 – integration time-dependent sources which are due to extraneous noise sources, *e.g.* the thermal generation of electron–hole pairs in the detecting volume of the CCD imager, or the equivalent background illumination noise generated in intensifiers (typically 2–3 equivalent photons $\text{s}^{-1} \text{mm}^{-2}$).

Type 3 – readout noise sources arise due to the final imperfect transfer of the integrated photo-induced charge and the additional noise sources present in the subsequent signal-processing chain. For a fixed processing chain, this contribution to the overall noise level is unaffected by the signal levels or integration times.

It is the magnitude of this type 3 noise that dictates the need or otherwise for prestorage gain to achieve satisfactory low-level signal performance. For cooled detectors, type 2 sources are not significant. If the integrated charge generated by a single detected photon is at least 5σ , where 5σ is the standard deviation of the probability density function of the total type 3 noise, then there is a greater than 99.99% probability of being able to detect this single event (assuming that the noise sources obey a stationary Gaussian process). If this is the case, there is no need to employ prestorage gain. In fact, its presence will adversely affect the dynamic range of the system (as the saturation limit will be reached earlier) and it will introduce additional type 1 and type 2 noise sources.

These arguments can be simplified if there are other reasons for including elements such as image intensifiers in specific applications – such as where there is a need for high magnification or demagnification; or if very fast signal gating is required. The schematic section of a structured scintillator–fibre-optic taper–CCD detector unit is shown in Fig. 3.

3.4. Optical relay: lens or fibre optics

The two choices are either a high-quality lens system or coherent fibre-optic faceplate or taper. The main requirement is to maintain a high transmission efficiency, and this need means that only small demagnification factors are feasible. For an ideal lens system, the light-collection efficiency is equal to the fraction of light subtended at the lens. The output of either a phosphor or scintillator screen, or the output of an intensifier, is approximately Lambertian. The efficiency, T_L , of a lens is given by,

$$T_L = 1/[1 + 4f^2(D_m + 1)^2], \quad (4)$$

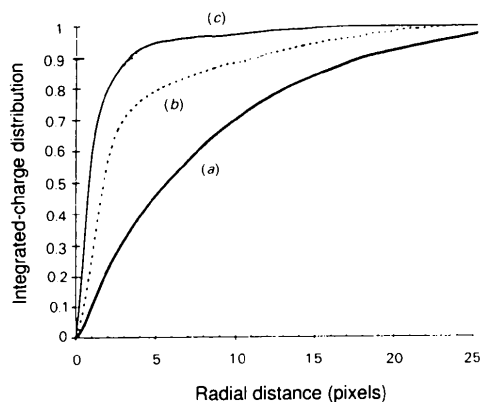


Figure 2

Integrated-charge collection profiles of the fibre-optic faceplate and CCD combination for (a) unstructured and (b) structured CsI(Tl) scintillator screens (30 μm thick: measured at $E_i = 8$ keV), and (c) fibre optic and CCD only (measured using visible light). The CCDs linear pixel dimension is 22 μm .

where f is the f -number of the lens and D_m is the demagnification factor. Real lenses will exhibit lower efficiencies due to reflection losses and the effects of vignetting. Table 2, based on Coleman (1985), shows the measured transmission efficiencies of typical lenses and fibre-optic tapers. The clear advantages of tapers are obvious. For quantum-limited performance with a non-intensified detector system, the maximum demagnification factor is about three. Higher demagnification factors will result in an unacceptable loss of scintillator light output. There is also a practical demagnification limit for tapers due to the restrictions on how fine bundled fibres can be pulled. As typical CCD areas are 10×10 to 20×20 mm, an overall system demagnification factor of at least ten would be required if a single CCD is to be used and the active aperture maintained at, say, 200×200 mm. Such single-stage reduction employing a lens or a taper is not practical. Either the intensifier (if present) must produce some demagnification or a mosaic of CCDs must be used (Westbrook, 1988). Fig. 4 shows such an arrangement of CCD modules. There are a number of advantages in such an approach. The restrictions on tiling mentioned in §3.1 are no longer present as the demagnifying tapers permit the use of conventional CCD packaging. Coherent demagnifying tapers are available from a small number of manufacturers and they can be accurately ground to the appropriate square profile. The 'imaging loss' at the taper boundaries can be reduced to a few pixels in width. The numerous small CCDs can be read out in parallel and so reduce the system's deadtime (or the readout rate reduced to limit the signal-processing chain's bandwidth and so

Table 2

Transmission efficiencies of typical lenses and fibre-optic tapers based on Coleman (1985).

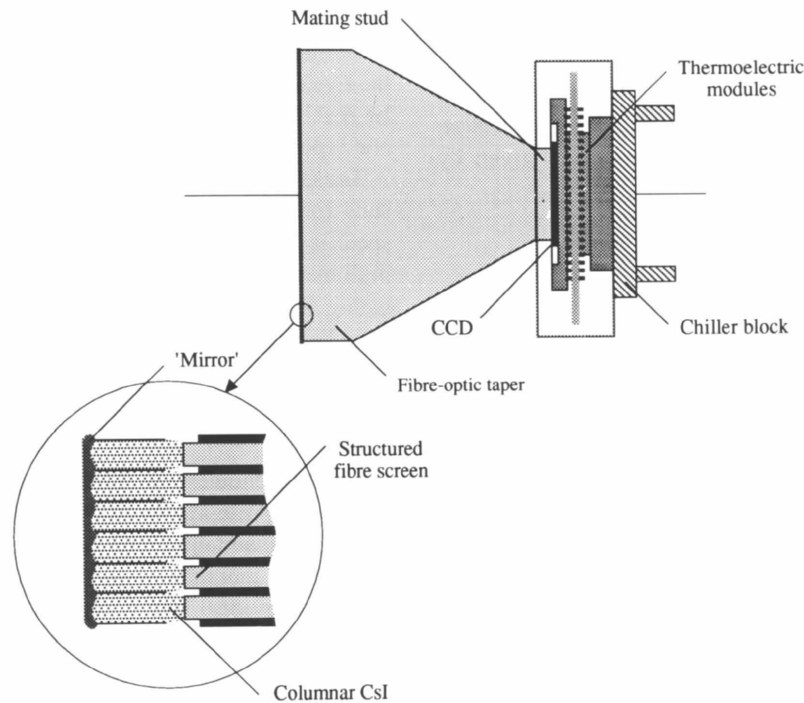
Demagnification factor	Ideal (%)	Lens (%)	Taper (%)
1	100	12	80
2.5	25	5	20
10	1	0.75	0.1

improve low-level performance). This modular approach also eases the development of large area systems.

The number of incident fibres per CCD photosite needs to be high in order to eliminate any sampling effects. The adhesive layer used to mount a fibre-optic bundle directly to the surface of the CCD needs to be very thin. For $2 \mu\text{m}$ fibres and a photosite of $20 \mu\text{m}$, there is a very serious reduction in resolution if this layer is thicker than about $5 \mu\text{m}$. Ideally, the layer should be less than $1 \mu\text{m}$, which imposes a strict specification for the flatness of the CCD die. Some CCDs (notably those made by Tektronix, Inc.) exhibit a prominent overall bulge in the CCD die. In such cases the face of the taper has to be accurately ground to a matching profile.

4. System characterization

Detector systems are often specified in terms of such main parameters as detective quantum efficiency, point-spread function and dynamic range. The following sections describe these three main parameters for scintillator-coupled systems, and demonstrate the need to intimately relate

**Figure 3**

General schematic of scintillator-fibre-optic taper-CCD detector module. The structured CsI scintillator is grown directly onto the prepared entrance aperture of the taper. A separate 1:1 fibre-optic mating stud is employed to ease manufacturing demands.

characterization to the particular detector topology and the intended application.

4.1. Detective quantum efficiency

4.1.1. *Definitions.* The most widely quoted parameter for any integrating detector system is its detective quantum efficiency. The effectiveness of any imaging detector is determined by its detection efficiency. The quantum efficiency, QE, is defined as,

$$QE = \frac{\text{mean number of detected electrons}}{\text{mean number of incident photons}} \text{ per photosite.} \quad (5a)$$

Detected electrons are the photo-generated electrons that are generated within the interacting volume of a photosite, collected and successfully transferred out of the detector. In the X-ray region, multiple electron-hole pairs are generated per interacting photon, so a more useful parameter is the detective quantum efficiency, DQE, namely,

$$DQE = \frac{\text{mean number of detected photons}}{\text{mean number of incident photons}} \text{ per photosite.} \quad (5b)$$

Note that both definitions are expressed in terms of an individual photosite.

These two expressions are related by,

$$QE = \eta_e DQE, \quad (5c)$$

where η_e is the effective quantum yield of the detector. η_e is always less than η_i , due to various internal loss mechanisms within the detector.

An alternative definition of DQE, based on the ratio of the input and output signal-to-noise ratios, can be derived as follows. Because the integrated incident photon flux will obey Poissonian statistics, the input noise, σ_i , is given by

$$\sigma_i = (N_0)^{1/2}. \quad (6)$$

Hence, the input signal-to-noise ratio can be expressed as,

$$(S_i / \sigma_i) = (N_0)^{1/2}. \quad (7)$$

A similar argument can be applied to the detector system's output signal-to-noise ratio if the r.m.s. deviation in the integrated number of detected electrons, N_D , obeys Poissonian statistics. Hence, we arrive at equation (1), which can be re-expressed as,

$$DQE = N_D / N_0. \quad (8a)$$

As some of the conversion processes in the detector chain do not obey Poissonian statistics, this relationship can be more accurately expressed as,

$$DQE = 1 / R_{\text{tot}} N_0, \quad (8b)$$

where the total system variance, R_{tot} , is the algebraic summation of the variances of additional noise sources and loss processes through the entire detecting chain.

Another useful parameter is the dose uncertainty, ρ , as this expresses explicitly the precision to which a particular measurement can be made,

$$\rho = (R_{\text{tot}})^{1/2} = 1 / (N_0 DQE)^{1/2}. \quad (9)$$

For an ideal detector system, *i.e.* one where all incident photons are detected, the resulting electrons are successfully transferred out of the detector and for which the detector introduces no additional noise sources or loss processes of its own, then the $DQE = 1$ and hence,

$$\rho = 1 / (N_0)^{1/2}. \quad (10)$$

The following analysis is concerned solely with a non-intensified scintillator-coupled CCD system. For a more general analysis, see Kalata, Stanton & Phillips (1992). The total system variance is given by,

$$R_{\text{tot}} = \left(\frac{\sigma_o}{S_o} \right) = R_0 + \frac{1}{N_0} \left[R_s + \frac{1}{g_s} \left(R_{\text{opt}} + \frac{R_{\text{ccd}}}{T_f} \right) \right] + R_\eta \quad (11)$$

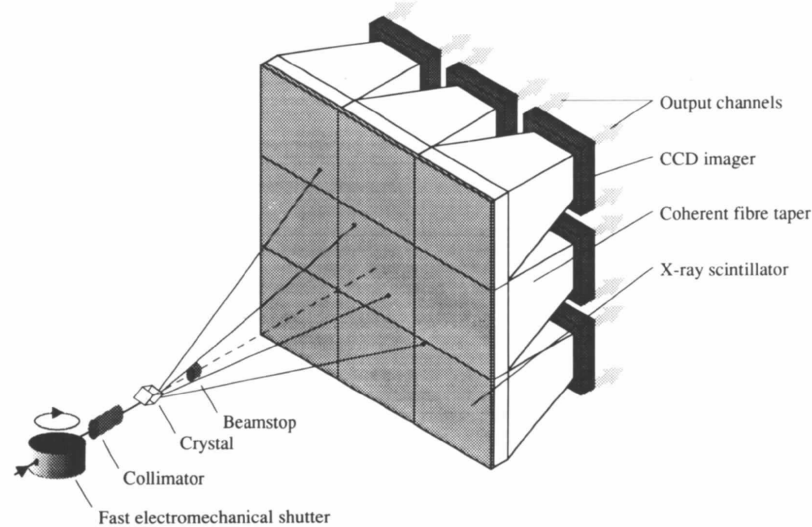


Figure 4

Example of a typical 3 × 3 mosaic CCD detector. The full active aperture of this system is approximately 150 × 150 mm. All the CCDs can be read out in parallel, with typically four output channels per device. Adapted from Westbrook (1988).

where

Variable	Relative variance	Distribution type
R_0 Number of detected photons	$\frac{1}{\varepsilon N_0}$	Poisson
R_s Number of scintillator photons	$\frac{1}{g_s}$	Poisson
R_{opt} Number of photons transmitted by optical relay	$\frac{1}{T_f} - 1$	Binomial
R_{ccd} Number of photons detected by CCD	$\frac{1}{\eta_{ccd}} - 1$	Binomial
R_η Detector system noise referred to input	$\frac{\eta_{eff}^2}{N_0^2}$	Poisson

and g_s is the mean scintillator gain, in visible photons per detected X-ray photon; N_0 is the incident signal, in photons; ε is the scintillator absorption; T_f is the transmission efficiency of the optical relay; η_{ccd} is the equivalent CCD noise (due to all components); and η_{eff} is the equivalent detector noise, which is the ratio of the r.m.s. detector noise to the signal produced for a single X-ray photon incident on the detector.

The energy deposited by each X-ray interaction in the scintillator is not constant and will be distributed according to some energy distribution. For this reason, scintillator-based systems are unsuitable for energy-discriminating applications. The signal-to-noise ratio of the scintillator will be modified by relating the ratio for a broad spectrum to that of a line spectrum (Swank, 1973). Namely,

$$\text{Signal/noise} = (\varepsilon N_0 A_s)^{1/2}, \quad (12)$$

where the parameter A_s , the absorbed energy distribution moment, is defined as,

$$A_s = M_1^2 / M_0 M_1, \quad (13)$$

where M_k is the k th moment of the pulse-height distribution given by

$$M_k = \sum_i n(E)_i E_i^k. \quad (14)$$

Hence, the system DQE can be expressed as,

$$\text{DQE} = \frac{1}{N_0} \left[\frac{1}{\varepsilon N_0} + \left(\frac{1}{g_s} + \frac{1}{A_s} - 1 \right) \frac{1}{\varepsilon N_0} + \left(\frac{1}{T_f} - 1 \right) \frac{1}{\varepsilon N_0 g_s} + \left(\frac{1}{\varepsilon_{ccd}} - 1 \right) \frac{1}{\varepsilon N_0 T_f} + \frac{\eta_{eff}^2}{N_0^2} \right]^{-1}. \quad (15)$$

This expression can be simplified if the variance contributions due to CCD and optical elements are negligible, to give

$$\text{DQE} = \varepsilon A_s N_0 / (N_0 + \varepsilon A_s \eta_{eff}^2). \quad (16)$$

This expression is similar to that given by Gruner, Milch & Reynolds (1978), except that the absorbed fraction is modified by the A_s term.

4.1.2. *Typical system performance.* The relative dose uncertainty can be determined for a typical system as a function of the incident X-ray dose. The physical noise sources associated with the CCD are the dark-current noise (due to the thermal generation of electron-hole pairs) and the readout noise (due to the uncertainty of resetting the potential of the output reset gate electrode). At an operating temperature of 193 K, the dark-current noise can be neglected as it is typically equivalent to 1 e r.m.s. per pixel over a 100 s integration period. For longer integration times, the operating temperature has to be reduced further (bulk dark current halves for approximately every 9 K reduction in the device temperature). The readout noise can effectively be eliminated by employing correlated double-sampling techniques. The system noise, which is proportional to the bandwidth of the subsequent signal-processing chain, is typically 40 e r.m.s. for a readout pixel rate of 500 kHz. This readout rate results in a total readout time of 500 ms for a typical 1000 × 1000 element CCD with four output amplifiers. Measurements on a 30 μm CsI(Tl) scintillator layer yield an absorption efficiency of 98% at $E_{hv} = 8$ keV; and for a 2.5:1 reducing optical taper an overall transmission efficiency of 11% has been obtained. The spectral match of the scintillator emission and the sensitivity of a standard front-illuminated CCD gives an integrated detection efficiency of 57%. The measured relative-dose uncertainty curve for this detector system is shown in Fig. 5, which also shows the theoretical curve for an *ideal* noiseless detector (DQE = 1) and for further comparison the calculated curve for a front-illuminated CCD detector system employing a 10:1 reducing lens as the optical relay. The results obtained can be improved slightly at low flux levels through the use of a back-illuminated CCD, and this calculated curve is also shown in Fig. 5. These representative curves illustrate the importance of high-efficiency optical coupling with low demagnification factors and the highest visible sensitivity for the CCD. For a total incident X-ray photon count of 100 photons, then the DQE is 0.53 for the front-illuminated CCD and 0.79 for a comparable back-illuminated device.

4.2. Point-spread function

An important parameter for all macromolecular crystallography applications is the PSF. Specifying the PSF at FWHM is of little value: a more realistic parameter would be at the 1%, or lower, of maximum intensity. The PSF of most detector systems exhibit long low-level intensity tails. Simple profiles of the PSF are deceptive as it is the integrated charge collected radially that is important, as Fig. 2 illustrates.

The lateral diffusion of the scintillator light in the system components has a major effect on the low-level performance of the entire detector system. As the induced charge in the CCD is spread over several pixels, and each pixel has associated with it a noise component, then the probability of accurately summing the induced charge is much reduced.

A criterion for the unambiguous detection of an event is that the signal must be at least 5σ , where σ is the r.m.s. noise level. If, for example, the induced charge is 10 e, and the r.m.s. noise per pixel is 1 e, then if this charge is deposited in a single pixel, the charge could be detected without difficulty. If, however, the charge is distributed across several pixels, then it could not be detected. The DQE calculations need to be modified to account for these effects. Fig. 6 shows the increased dose uncertainty at low dose levels based on Monte-Carlo simulations of a typical

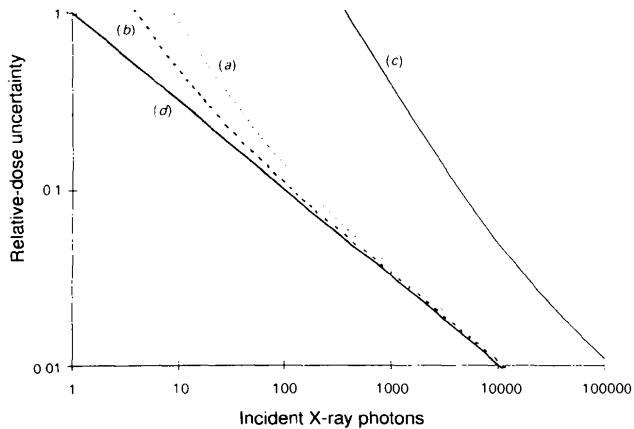


Figure 5

(a) Measured relative-dose uncertainty curve as a function of incident X-ray photon dose for a prototype system employing a $30\ \mu\text{m}$ structured CsI:Tl scintillator on a 2.5:1 reducing fibre-optic taper. There will be a slight improvement at very low dose levels if a back-illuminated CCD is used in place of the more conventional front-illuminated variety. The predicted curve is shown as (b). The poor estimated performance for a system employing a 10:1 reducing lens as the optical relay is shown as curve (c). The following parameters are used: photon energy, 8 keV; total system noise, 45 e r.m.s., scintillator efficiency, 11%; scintillator absorption, 98%. The response for an ideal detector (DQE = 1) is shown as curve (d).

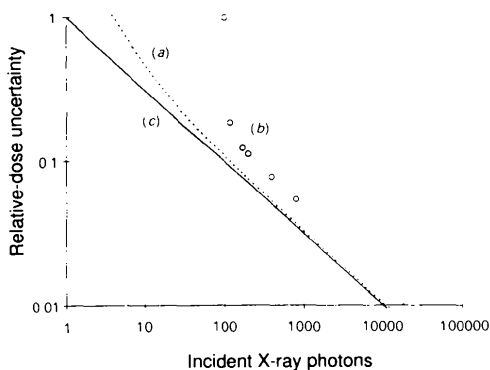


Figure 6

Calculated relative-dose uncertainty curves as a function of incident X-ray photon dose when the effects of the beam collimation and the PSF of the detection system are taken into account. The detector PSF is assumed to be that of a structured scintillator and with 2×2 on-chip pixel binning operative; otherwise all other parameters as in Fig. 5. (a) Not corrected for PSF effects; (b) Corrected for PSF effects; (c) Ideal detector.

scintillator–fibre taper–CCD system (Castelli & Allinson, 1994). This effect has been observed in similar systems (Gruner *et al.*, 1993), and can give rise to unrealistically high DQE estimates at low flux levels. It should be stressed that these effects will be present in all tessellated detector systems (including image-plate systems) and will be particularly severe where the PSF exhibits extended tails.

4.3. Dynamic range

The dynamic range of a detector system has a number of differing definitions. It is often quoted as the ratio of the saturation level of the detector (*i.e.* the level at which the responsivity of the detector becomes non-linear) to its mean noise floor. For example, a typical slow-scan CCD detector may possess an r.m.s. noise level of 10 e and a saturation charge of 10^6 e (*i.e.* when the photosite well is full and any further induced charge will result in charge spreading to neighbouring photosites) – hence the dynamic range is quoted as $10^5:1$. The assumption, inherent in this definition, is that the minimum detectable signal is equal to the mean noise level. This is appropriate if signal-averaging techniques are used to recover the signal from the incoherent background noise. Dynamic range can be more usefully expressed in terms of the range of meaningful measurements that can be obtained, and hence any definition will be dependent on a specific application. For crystallographic applications, the detector's dynamic range can be defined as,

Dynamic range =

$$\frac{\text{Integrated spot intensity that just saturates the detector}}{\text{Integrated spot intensity at minimum acceptable accuracy}} \quad (17)$$

This parameter needs to be quoted for a single integration period, and this period is defined in terms of the minimum integration time needed to acquire the integrated intensity of a typical spot to a pre-specified accuracy. For the examples given in Table 3, the typical spot intensity was taken as $100\ \text{photons s}^{-1}$ and measured to 3% accuracy. The minimum acceptable spot intensity accuracy was taken as 10%. These parameters are to some extent arbitrary but they do reflect practical constraints set by crystallographers. Three spot profiles are chosen to illustrate the major effect of profile on dynamic range. They are defined as,

(a) Perfect top-hat profile with a diameter of $300\ \mu\text{m}$.

(b) Pure Gaussian profile with a FWHM of $300\ \mu\text{m}$, and the boundary radius taken to where the spot profile is 2% of peak.

(c) Realistic profile with a $300\ \mu\text{m}$ diameter rectangular profile convoluted with an effective $100\ \mu\text{m}$ FWHM Gaussian PSF, and the boundary radius as defined in (b).

These calculated figures indicate that not only can high dynamic range be obtained from CCD detectors but that care should be taken, by experimenters, to ensure that incident spot profiles are optimized. Defining dynamic range

Table 3

Estimates of dynamic range for a typical scintillator–fibre-optic taper–CCD detector.

Spot profile	Wavelength (Å)	Integration time (s)	Dynamic range (N:1)
Top hat	0.9	15	8700
	0.7	20	7700
	0.5	37	6100
Gaussian	0.9	19	5200
	0.7	24	4800
	0.5	43	4200
Realistic	0.9	16	6400
	0.7	21	5800
	0.5	39	4900

Notes: (1) Integration time set to ensure 3% accuracy for a nominal 100 photons s^{-1} spot. (2) Saturation level set by 5×10^5 e CCD full well capacity. (3) Minimum measurable spot intensity set by 10% accuracy taking into account the system noise floor.

simply in terms of the CCDs saturation level and noise floor (for this system 5.5×10^5 e and 22 e, respectively) would have yielded the much higher value of 23×10^3 , but this would not be representative of attainable data. By incorporating the spot profile and the PSF for the detecting system, it is then possible to compare directly the attainable quality of crystallographic data for differing experimental arrangements and detectors.

5. Conclusions

Both the practical and modelling results presented here show that it is possible to develop large area detectors, based on scintillators or phosphors closely coupled through fibre optics to CCDs, to meet the stringent requirements of macromolecular crystallography. A mosaic of closely coupled, reducing fibre-optic tapers allow the construction of a very large aperture detector system with minimal loss of aperture coverage and high-speed readout. The latter is particularly important as increased incident fluxes become available and there is a growing interest in dynamic crystallographic experiments. The essential requirement is a high-gain primary converter with minimal PSF (in particular the absence of long tails). The importance of maintaining the highest possible spatial resolution throughout the detecting chain is crucial if high DQE is to be obtained for low-level signal operation. It is possible, however, to provide quantum-limited detection systems. The interrelationships between the various system parameters have been stressed and these parameters should be expressed in terms of the intended applications. CCD-based detector systems are beginning to show their true potential (and not just for macromolecular crystallographic applications), and without doubt they will play a major part in the scientific exploitation of synchrotron radiation sources over the coming decade.

This work has been generously supported by grants from the EC Science Plan (reference ERBSC1 CT000269-XC1000269) and EPSRC (reference GR/H 62084 and GR/J

78297). The SERC Daresbury Laboratory is thanked for the provision of synchrotron radiation facilities. EEV (Chelmsford) have been especially supportive over many years; in particular the assistance of J. E. U. Aston, I. T. Flint and P. J. Pool is acknowledged. All the hard work is due to the efforts of the group members at York, namely C. M. Castelli, B. G. Magorrian and K. J. Moon. I also wish to acknowledge the many helpful discussions with numerous colleagues, especially J. R. Helliwell (Manchester), G. E. Derbyshire and C. Nave (Daresbury), and K. Wilson (Hamburg). Thanks are also firmly in order to the small, but important, group of dedicated detector developers around the world for their mutual help and support.

References

- Allinson, N. M., Allsopp, D. W. E., Quayle, J. A. & Magorrian, B. G. (1991). *Nucl. Instrum. Methods*, **A310**, 267–272.
- Allinson, N. M., Carr, P. D., Colapietro, M., Harding, M. M., Helliwell, J. R., Thompson, A. W. & Weisgerber, S. (1989). *J. X-ray Sci. Technol.* **1**, 143–153.
- Allinson, N. M., Colapietro, M., Helliwell, J. R., Moon, M. J., Thompson, A. W. & Weisgerber, S. (1992). *Rev. Sci. Instrum.* **60**, 664–666.
- Amemiya, Y., Yagi, N., Kishimoto, S., Oguchi, T., Suzuki, M., Ohnishi, Y. & Wakabayashi, K. (1994). *Developments of X-ray Television Detectors at the Photon Factory*. In *Synchrotron Radiation in Bio-Science*. Oxford Univ. Press.
- Arbel, A. F. (1980). *Analog Signal Processing and Instrumentation*, p. 351. Cambridge Univ. Press.
- Arndt, U. W. (1986). *J. Appl. Cryst.* **19**, 145–163.
- Arndt, U. W. (1990). *Synchrotron Rad. News*. **3**, 17–22.
- Castelli, C. M. & Allinson, N. M. (1994). *Opt. Eng.* Submitted.
- Castelli, C. M., Allinson, N. M., Moon, K. J. & Watson, D. L. (1994). *Nucl. Instrum. Methods*. Submitted.
- Coleman, C. I. (1985). *Adv. Electron. Electron Phys.* **64**, 649–655.
- Eikenberry, E. F., Tate, M. W., Bilderback, D. H. & Gruner, S. M. (1992). *X-ray Detectors: Comparison of Film, Storage Phosphors and CCD Detectors*. In *Photoelectric Image Devices*, edited by B. L. Morgan, pp. 273–280. Bristol: IOP Publishing.
- Gruner, S. M. (1989). *Rev. Sci. Instrum.* **60**, 1545–1551.
- Gruner, S. M., Barna, S. L., Wall, M. E., Tate, M. & Eikenberry, E. F. (1993). *Proc. Soc. Photo-Opt. Instrum. Eng.* **2009**, 98–108.
- Gruner, S. M., Milch, J. R. & Reynolds, G. T. (1978). *IEEE Trans. Nucl. Sci.* **25**, 562–565.
- Helliwell, J. R. (1992). *Macromolecular Crystallography with Synchrotron Radiation*. Cambridge Univ. Press.
- Ito, M., Yamaguchi, M. & Oba, K. (1987). *IEEE Trans. Nucl. Sci.* **34**, 401–405.
- Janesick, J. & Elliott, T. (1992). *History and Advancements of Large Area Scientific CCD Imagers*. In *Astronomical CCD Observing and Reduction Techniques*, ASP Conference Series Vol. 23, edited by S. B. Howell, pp. 1–67. San Francisco: Astronomical Society of the Pacific.
- Kalata, K., Stanton, M. & Philips, W. (1992). *J. X-ray Sci. Technol.* **3**, 157–165.
- Magorrian, B. G. & Allinson, N. M. (1988). *Nucl. Instrum. Methods*, **A273**, 500–604.
- Phillips, W., Stanton, M., O'Mara, D., Naday, I. & Westbrook, E. (1993). *Proc. Soc. Photo-Opt. Instrum. Eng.* **1900**, 53–58.
- Swank, R. K. (1973). *Appl. Opt.* **12**, 1865–1872.
- Westbrook, E. M. (1988). Conceptual Design Report Document No. J9001-2001-SA-01. Argonne National Laboratory, Illinois, USA.